Title
Kinetics of IO Production in the CH2I + O2 Reaction Studied by Cavity Ring-Down Spectroscopy

Journal
The Journal of Physical Chemistry A, 119(34)

ISSN
1089-5639

Authors
Foreman, Elizabeth S
Murray, Craig

Publication Date
2015-08-27

DOI
10.1021/acs.jpca.5b05058

Peer reviewed

Kinetics of IO Production in the $CH_2I + O_2$ Reaction Studied by Cavity Ring-Down Spectroscopy

Elizabeth S. Foreman and Craig Murray*

Department of Chemistry, University of California, Irvine, Irvine CA 92697, USA

* Email: craig.murray@uci.edu; Telephone: +1-(949)-824-4218

Abstract

Cavity ring-down spectroscopy has been used to study the kinetics of formation of IO radicals in the reaction of $CH_2I + O_2$ in a flow cell at 52±3 Torr total pressure of N_2 diluent and a temperature of 295 K. CH_2I was produced by photolysis of CH_2I_2 at 355 nm and IO probed on the $A^2\Pi_{3/2}$–$X^2\Pi_{3/2}$ (3,0) and (3,1) bands at 435.70 and 448.86 nm, respectively. The rates of formation of IO(v''=0) and IO(v''=1) have been measured as a function of O_2 number density using either conventional transient absorption or the simultaneous kinetic and ring-down (SKaR) technique, respectively. IO(v''=1) was found to be formed with a significantly larger rate constant, but reached far smaller peak concentrations than IO(v''=0). Kinetic modeling supports the conclusion that IO(v''=0) is produced both directly and through secondary chemistry, most probably involving the initial formation of the Criegee intermediate CH_2OO and subsequent reaction with I atoms, while IO(v''=1) is produced exclusively via a direct mechanism. We propose that the reaction mechanism (direct or indirect) depends upon the degree of initial excitation of the photolytically-produced CH_2I reagent.

Introduction

Organoiodides, emitted primarily from oceanic sources, are well established precursors to radical-initiated catalytic ozone depletion and to new particle formation in the troposphere.[1–3] Iodine atoms are formed primarily by photolysis and react promptly with ozone to form IO, resulting in an average ozone loss rate of 1.67–3.38 ppb per day.[4] Concentrations of IO on the order of 10^8 cm^{-3} (approximately 100 times greater than average OH radical concentration) near coastal areas may also significantly affect the oxidative potential of the atmosphere, as evidenced for example by a rate constant for the oxidation of DMS that is competitive with that by OH radicals.[5] Subsequent self-reaction of IO leads to higher order iodine oxides (I_xO_y) which have been linked to particle formation and aerosol growth.[3]

Diiodomethane (CH_2I_2) is the largest organoiodide contributor to I atom flux in the marine boundary layer. CH_2I_2 dissociates promptly after absorption in the near UV; the absorption spectrum extends as far as ~360 nm, approximately 80 nm further into the actinic region than the most abundant organoiodide, iodomethane (CH_3I). Consequently, the atmospheric lifetime of CH_2I_2 is calculated to be only a few minutes,[6,7] while that of CH_3I is several days.

$$CH_2I_2 + h\nu \rightarrow CH_2I + I \qquad \Delta H = 56.4 \text{ kcal mol}^{-1} \qquad (1)$$

CH_2I radicals can subsequently produce reactive iodine species either by secondary photolysis, or more probably, by reaction with O_2.

$$CH_2I + O_2 \rightarrow \text{products} \qquad (2)$$

Both CH_2I_2 and CH_3I produce iodomethyl radicals in the atmosphere – the former by direct photolysis and the latter by reactions with OH or Cl. While the relatively slow photolysis is the dominant loss process for CH_3I, the abstraction reactions with OH (and to some extent Cl atoms)

to form iodomethyl radicals is not insignificant, accounting for 10–20% of the total removal.[8] Reaction (2) has been a subject of some interest, as it can regenerate reactive iodine species in the atmosphere. More recently, it has been widely used as a source of stabilized Criegee intermediates in laboratory studies, in preference to the highly exothermic ozonolysis of unsaturated hydrocarbon species. Reaction (2) can proceed via three pathways, which can lead to either reactive iodine species or stabilized peroxyiodomethyl radicals:

$$CH_2I + O_2 \rightarrow HCHO + IO \qquad \Delta H = -48 \text{ kcal mol}^{-1} \qquad (2a)$$

$$CH_2I + O_2 \rightarrow CH_2OO + I \qquad \Delta H = -1 \text{ kcal mol}^{-1} \qquad (2b)$$

$$CH_2I + O_2 + M \rightarrow CH_2IO_2 + M \qquad \Delta H = -29 \text{ kcal mol}^{-1} \qquad (2c)$$

While most kinetics studies of reaction (2) have been carried out at or close to room temperature, the experimental conditions have been otherwise highly dissimilar, using different means of producing CH_2I radicals and spanning a range of pressure conditions. The detailed mechanism remains somewhat uncertain. Photoionization mass spectrometry (PIMS) studies of the loss rate of CH_2I by Masaki *et al.*[9] and Eskola *et al.*[10] at low pressure (<15 Torr) produced rate constants reaction (2) of $k_2 = (1.6\pm0.2)\times10^{-12}$ cm^3 s^{-1}(95% confidence limit), and $(1.37\pm0.32)\times10^{-12}$, respectively. All errors reported here represent 1σ uncertainty unless otherwise indicated. In contrast to the analogous reaction of CH_2Br with O_2, for which falloff behavior was observed,[10] reaction (2) was found to display no pressure dependence. Eskola *et al.* estimated the yield of I atoms to be near unity, while the yield of HCHO was estimated to be less than 0.33.[10] There have been several kinetic studies monitoring the formation of IO as a product of reaction (2), but significant discrepancies exist between the measured rate constants. Enami *et al.* used cavity ring-down spectroscopy to study the kinetics of IO formation after generating CH_2I radicals by photolysis of CH_2I_2 at 266 nm.[11] Transient absorption measurements of IO formation resulted in

a bimolecular rate constant of $k_{2a} = (4.0\pm0.4)\times10^{-13}$ cm^3 s^{-1} and an assumed IO yield of unity. The lack of pressure dependence of the IO yield and rate constant between 5–80 Torr led to the conclusion that IO was produced directly via reaction (2a). A later cavity ring-down study by the same group used the hydrogen abstraction reaction between Cl + CH_3I to produce CH_2I radicals, with the aim of eliminating absorption of background I_2 formed from the recombination reaction of photolytically generated I atoms. These measurements resulted in a larger rate constant of $k_2 = (1.28\pm0.22)\times10^{-12}$ cm^3 s^{-1} (2σ uncertainty). The yield of IO from reaction (2) was reported to be 0.17±0.12 at 760 Torr, but around a factor of three larger in the zero-pressure limit.[12] Dillon *et al.* probed IO using laser-induced fluorescence and found an IO yield of < 0.12 at a total pressure of ~15 Torr and found evidence that IO formation was a result of secondary chemistry.[13]

Gravestock *et al.* used an array of techniques to examine reaction (2) over a range of experimental conditions and also concluded that IO was produced from secondary chemistry.[14] Their mechanism suggested that reaction between I atoms and the collisionally stabilized peroxyiodomethyl radical (CH_2IO_2) formed in reaction (2c) was the source of IO:

$$CH_2IO_2 + I \rightarrow HCHO + IO + I \qquad \Delta H = -19 \text{ kcal mol}^{-1} \qquad (3)$$

The rate of IO formation was found to depend linearly on both O_2 and CH_2I_2 number density, despite pseudo-first order conditions in which the O_2 number density was 17,000 times greater than that of CH_2I. This suggested an indirect formation mechanism involving the reaction of a "species X" with I atoms. By directly monitoring IO absorption at 30 Torr total pressure under two different O_2 number density regimes (<0.3% and 1–10% O_2 in N_2 balance), they found two different rates constants: $(1.0\pm0.3)\times10^{-13}$ and $(2.2\pm1.8)\times10^{-15}$ cm^3 s^{-1}, respectively. Monitoring the rate of formation of IO as a function of CH_2I_2 number density at constant O_2 produced a rate

constant of 3.8×10^{-11} cm^3 s^{-1} which was attributed to reaction (3). A rate constant of 2.6×10^{-14} cm^3 s^{-1} was estimated based on direct formation via reaction (2a) at atmospheric pressure, which was interpreted as evidence supporting the indirect mechanism due to the discrepancy with earlier measurements. Further evidence supporting IO formation via secondary reactions was the identification of the absorption spectrum of "species X" at 275–425 nm to CH_2IO_2, following an earlier assignment by Sehested *et al*.[15] In light of more recent work, however, it seems likely that the spectrum was in fact the $\tilde{B}^1A'$–$\tilde{X}^1A'$ transition of the carbonyl oxide biradical, or Criegee intermediate, CH_2OO.[16–18] No direct experimental evidence has been found for the CH_2IO_2 radical in ionization studies.[10,14]

Application of the $CH_2I + O_2$ reaction to the laboratory synthesis of CH_2OO via reaction (2b) has prompted new interest in reaction (2). In the atmosphere, ozonolysis of alkenes produce a stable carbonyl fragment and a highly internally excited Criegee intermediate fragment in a process that is exothermic by 48.8 kcal mol^{-1}. Criegee intermediates remained particularly elusive in the gas phase until Welz *et al.* demonstrated the use of VUV ionization mass spectrometry.[19,20] In contrast to ozonolysis, reaction (2b) is only very mildly exothermic and results in stable and hence readily detectable Criegee intermediates. This development has led to the direct spectroscopic detection of CIs in the ultraviolet, infrared, and microwave regions.[17,18,21,22] CH_2OO is formed rapidly and branching for reaction (2b) appears to be significant, although reported yields vary.[23–25] In light of the rapid formation of CH_2OO, an alternative indirect reaction mechanism for the formation of IO is:

$$CH_2OO + I \rightarrow HCHO + IO \qquad \Delta H = -47 \text{ kcal mol}^{-1} \qquad (4)$$

In a detailed study of the $CH_2I + O_2$ reaction, Ting *et al.* ascribed the formation of IO to reaction (4) at total pressures below 60 Torr and to reaction (3) at higher pressures where the collisional

stabilization of CH_2IO_2 is thought to be significant.[25] An assumed pressure-independent rate constant of $k_4 = 9.0\times10^{-12}$ cm^3 s^{-1} was found to be necessary in the kinetic model to describe the IO formation rate, although this is almost 200 times larger than the rate predicted from *ab initio* calculations characterizing the transition state.[26]

In this work, we report on the kinetics of IO formation in the reaction of photolytically-generated CH_2I with O_2 using cavity ring-down spectroscopy (CRDS). IO radicals were probed on the $A^2\Pi_{3/2}$–$X^2\Pi_{3/2}$ transition and found to be formed in both v''=0 and v''=1. IO(v''=1) appears to be formed via a direct mechanism, and the rate constant decreases with increasing total pressure. Interestingly, while the apparent rate constant for IO(v''=0) around five times smaller than that of IO(v''=1), the yields are approximately 0.10 and 0.01, respectively. A kinetic model of the CH_2I + O_2 reaction suggests that IO(v''=0) is formed via direct and sequential mechanisms involving secondary reactions. The rate constant for vibrational relaxation of IO(v''=1) by N_2 is also determined and found to be a negligible contributor to the formation of IO(v''=0). The effect that the degree of internal excitation of the CH_2I radicals produced in the photolysis of CH_2I_2 has on the detailed mechanism is discussed.

Experimental

The reaction between CH_2I and O_2 was studied in a small stainless steel flow cell. CH_2I radicals were generated by the photolysis of CH_2I_2 precursor and the resulting IO products were detected by cavity ring-down spectroscopy. N_2 (Praxair, THC free, 99.998%) is bubbled through the precursor CH_2I_2 (Sigma-Aldrich, 99%) and O_2 (Praxair, THC free, 99.99%) is added to the flow before entering the reaction flow cell. All gas flows were regulated by calibrated mass flow controllers (Alicat) to give a total volumetric flow rate of ~1.7 slpm. The total pressure was monitored with a Baratron pressure transducer (MKS) and controlled by throttling the valve

connected to a rotary vane pump (Leybold Oerlikon D16B). The ring-down mirrors that form the optical cavity along the long axis of the flow cell are purged with a small flow of N_2 to prevent damage to the mirror coatings

CH_2I radicals were generated by the photolysis of CH_2I_2 using the third harmonic of an Nd:YAG laser (Continuum Surelite II) at 355 nm. The unfocused photolysis laser beam was steered into the flow cell through a quartz window orthogonal to the probe axis, resulting in an interaction length of approximately 6 mm, the diameter of the photolysis beam. The photolysis pulse energy is attenuated to achieve a fluence of approximately 57 mJ cm^{-2}. Using an absorption cross section for CH_2I_2 at 355 nm of 2.05×10^{-19} cm^2, we estimate that ~2% of the CH_2I_2 molecules are dissociated giving an initial CH_2I number density of $4\pm1\times10^{14}$ cm^{-3}.[27] The IO products of the $CH_2I + O_2$ reaction are probed using cavity ring-down spectroscopy. First introduced by O'Keefe and Deacon in 1988,[28] CRDS has become a workhorse for trace-level gas phase linear absorption studies in recent years due to the high sensitivity and versatility of the technique.[29] A 5 ns pulse of light generated by Nd:YAG (Continuum Surelite III) pumped dye laser (Continuum ND6000, 0.08 cm^{-1} bandwidth) is coupled into the optical cavity comprising two highly reflective mirrors (CRD Optics, center λ = 440 nm, nominal R = 0.9996) separated by 37.5 cm. The dye laser was operated with Coumarin 440 dye and the pulse energy was attenuated to <20 μJ $pulse^{-1}$. With each pass, a small fraction of each pulse is lost by transmission through the ring-down mirrors resulting in an exponential decay with a lifetime of ~3 μs. The light transmitted through the rear mirror is collected with a PMT and is digitized by a high-resolution 12-bit, 500 MHz digital oscilloscope. Waveforms were transferred to a PC running LabView and fit to single exponential decays in real time. A digital delay generator (Quantum Composers) is used to synchronize the photolysis and probe laser pulses.

Results

Spectroscopic Detection of IO

Absorption spectra of IO radicals were obtained by stepping the dye laser wavelength over known vibronic bands of the $A^2\Pi_{3/2}$–$X^2\Pi_{3/2}$ transition while simultaneously measuring the ring-down time, τ. The ring-down time is related to the absorption coefficient α by

$$\alpha = \frac{1}{c}\left(\frac{1}{\tau} - \frac{1}{\tau_0}\right) = \sigma(\lambda) n_{IO} \quad \text{(E1)}$$

where c is the speed of light, τ_0 is the empty cavity ring-down-time, $\sigma(\lambda)$ is the wavelength-dependent absorption cross section and n_{IO} is the number density of IO. A polynomial fit was used to model the empirical wavelength-dependence of τ_0 arising from variation in the mirror reflectivity.

The spectroscopy of IO has been relatively well characterized. The absorption spectrum of IO in the range 400–470 nm comprises a vibronic progression that converges beyond v'=6 into a broad, unstructured band. Resolvable rotational structure is observable only in some A–X bands, as rapid predissociation of the $A^2\Pi_{3/2}$ state leads to significant line broadening that is strongly dependent on the vibrational level.[30] In preliminary measurements, IO was detected on various A–X bands that fell within the range of wavelengths covered by near-optimum mirror reflectivity. Figure 1 shows normalized cavity-ring down absorption spectra of the IO A–X(3,0) and (3,1) bands, which have origins at 435.70 nm and 448.86 nm, respectively. Spectra were recorded by averaging 20−30 laser shots at each probe laser wavelength. To confirm the identity of the absorber, the IO A–X(3,0) and (3,1) bands were simulated in PGOPHER[31] using published spectroscopic constants.[30,32] The spectral linewidth in the simulations was determined by homogeneous lifetime broadening resulting from the 6.6 ps lifetime of the v'=3 level of the

electronically excited state. The A–X(3,1) band simulation contains a small contribution from high-*J* lines of the adjacent (2,0) band.

The experimental spectra clearly demonstrate the formation of vibrationally excited IO radicals in the $CH_2I + O_2$ reaction under the conditions of these experiments. We were unable to conclusively identify any transitions originating in higher vibrational levels of the ground state within the ~415−465 nm useful range of our ring-down mirrors. The (3,2) band located at 462.65 nm was not observed, likely due to its small Franck-Condon factor (3.88×10^{-3}). Transitions to higher vibrational levels such as the (5,2) band at 444.19 nm lack resolvable rotational structure and would be difficult to discern, particularly if the population in $v''=2$ were small. The peak absorption coefficient observed for the (3,0) band was larger than that for the (3,1) band, suggesting greater population in $v''=0$ than $v''=1$, although this depends upon the relative transition strengths and will be discussed later. The time delays between the photolysis and probe laser pulses required to optimize the absorption coefficients on the (3,0) and (3,1) bands were very different, however. Peak absorption was observed using delays of around 50 μs with the probe laser tuned to the (3,0) band head while around 6 μs was optimum for detection of the (3,1) band. IO radicals in $v''=0$ and $v''=1$ appear therefore to be formed with very different rates.

Kinetics of IO($v''=0$) formation

The time dependence of the number density of IO in its ground vibrational state was monitored with the probe laser tuned to the (3,0) band head, as indicated in Figure 1, while stepping the delay between the photolysis and probe lasers. Kinetic profiles, recorded with total pressure maintained at 52±3 Torr, and fraction of O_2 varied from 0.05−0.16, are shown in Figure 2. The absorption coefficient, which is directly proportional to the IO($v''=0$) number density, reaches a

maximum approximately 40–60 μs after the photolysis pulse. The growth period is ~20 times longer than the ring-down time, hence time profiles were measured by stepping the time delay between the photolysis and probe laser pulses. While this is likely to introduce some error at short delays, when the IO population is varying significantly over the ring-down time, the waveforms showed no significant non-exponential behavior. The loss of IO is significantly slower under these experimental conditions but the ring-down time does return to τ_0 on a timescale shorter than the 100 ms laser repetition period. IO removal is likely dominated by the self-reaction:

$$\text{IO} + \text{IO} \rightarrow \text{products} \tag{5}$$

for which $k_5 = 9.9\times10^{-11}$ cm^3 s^{-1}.[33,34] The diffusion coefficient for IO in an N_2 bath at 50 Torr and 295 K is 0.31 cm^2 s^{-1} which corresponds to a diffusion distance of only 0.066 mm in 70 μs (or 2.5 mm in 100 ms as an upper limit), considerably smaller than the probe beam diameter of ~6 mm. It is unlikely that either diffusion out of the probe region or wall losses would significantly affect the kinetic measurements.

Since the IO formation rate is ~30 times greater than the loss rate, reliable formation rates can be obtained by fitting only the rising edge of the time profile to a monotonic exponential rise to obtain a pseudo-first order rate constant, $k' = k_{2a,0} n_{O_2}$:

$$n_{\text{IO}}(t) = n_{\text{IO,max}}\{1 - \exp(-k't)\} \tag{E2}$$

Each data point is associated with a standard error of 4–6% resulting from the average of 30 ring-downs per time step. The average values of k' determined from five independent experiments are shown as a function of n_{O_2} in Figure 3 with vertical error bars representing the standard deviation between the repeat measurements, and horizontal error bars representing the

uncertainty in O_2 number density arising from fluctuations in the total pressure. All uncertainties reported here represent 1σ.

The IO(v''=0) formation rate, k', increases only modestly with O_2 number density, as shown in Figure 3. A linear fit yields a bimolecular rate constant for production of IO(v''=0) via reaction (2a) of $k_{2a,0} = (1.5\pm0.1)\times10^{-13}$ cm^3 s^{-1} (see Table 1) but does not pass through the origin, implying a measurable rate of IO formation even in the absence of O_2. This observation is interpreted as evidence that IO(v''=0) is not (or at least not exclusively) produced by a direct reaction mechanism and that the appearance of first order kinetics is misleading. Gravestock *et al*. observed a similar trend in their pseudo-first order rate constants in the "high O_2" regime, which would also lead to a non-zero intercept if extrapolated to $n_{O_2} = 0$.[14]

Kinetics of IO(v''=1) formation

The formation of vibrationally excited IO is rapid in comparison to that of the ground state, typically reaching a maximum in ~6 μs. The number density of IO(v''=1) consequently changes significantly within the duration of a ring-down event, which induces non-exponential behavior. Under these conditions, stepping the time-delay between the photolysis and probe laser is no longer a reliable means of measuring the reaction kinetics and the simultaneous kinetics and ring-down (SKaR) technique developed by Brown *et al.* has been implemented.[35,36] The SKaR method enables one to separate the kinetics of the absorbing species from the temporal characteristics of the empty cavity for processes occurring on timescales shorter than or comparable to the ring-down time. The ring-down waveform for a case where the concentration of the absorber is not constant over the ring-down time is given by:

$$I(t) = I_0 \exp\left(-\frac{t}{\tau_0} - c\sigma \int_0^t n_{IO}(t)dt\right) \quad \text{(E3)}$$

All reactions have been carried out under pseudo-first order conditions (large excess of O_2), and a monotonic exponential rise was assumed to model the time profile of n_{IO}. The kinetics of the absorber are represented by the ratio, $R(t)$, of the ring-down waveforms with and without absorbers present, $I(t)/I_0(t)$. The natural logarithm of the ratio is the SKaR profile that is fit to the experimental data and floating both k' and α_∞, where α_∞ represents the maximum absorption by IO after the reaction has been completed:

$$\ln R(t) = -\frac{c\alpha_\infty}{k'}\{k't - [1 - \exp(-k't)]\} \quad \text{(E4)}$$

In order to improve the robustness of the fit, α_∞ can be determined independently if need be and constrained in the two-parameter SKaR fit. In the long-time limit, $\ln R(t)$ reduces to the following expression, in which case α_∞ can be extracted from the slope of a linear fit:

$$\ln R(t) = -\frac{c\alpha_\infty}{k'}(k't - 1) \quad \text{(E5)}$$

Experimentally, ring-down waveforms are recorded in the presence or absence of absorbers by alternating the relative time delay between the photolysis and probe laser pulse. Firing the photolysis pulse 100 ns *after* the probe pulse ("photolysis on") results in a ring-down waveform that contains the time-dependent absorption of IO(v''=1). As such, the entire IO(v''=1) formation process could be captured within the 10 μs observation window provided by a ring-down time of ~3 μs. Delaying the photolysis pulse to fire 8 ms after the probe pulse ("photolysis off") provides the empty-cavity ring-down profile. Typically, 300 ring-down waveforms (150 photolysis on and 150 photolysis off) were accumulated in order to generate each SKaR profile.

Figure 4 shows SKaR profiles obtained after 355 nm photolysis of CH_2I_2 at a total pressure of 52±3 Torr. O_2 fractions ranged from 0.02−0.15 with N_2 balance. The probe laser was tuned near to the IO A–X(3,1) band head, selected specifically to avoid nearby (2,0) absorption lines.

Absence of ground state absorption in the signal at this wavelength was qualitatively verified by monitoring the absorption while stepping the time delay between photolysis and probe pulses using the method discussed in the previous section.

Fitting the SKaR profiles yields pseudo-first order rate constants for the formation of IO(v''=1) as a function of n_{O_2}, and the average reaction rates determined from at least five repeated experiments are shown in Figure 3 alongside the IO(v''=0) data. The rate of formation of vibrationally excited IO radicals also increases linearly with O_2 number density. In the case of IO(v''=1), however, the bimolecular rate constant was determined to be $k_{2a,1}$ = (9±1)×10^{-13} cm^3 s^{-1}, a factor of six larger than $k_{2a,0}$ (see Table 1) We tested that these results are not simply an artifact of the SKaR method by making conventional transient absorption measurements and found rate constants that agreed within their mutual uncertainties.

As an aside, we also used the SKaR method to measure the first 10μs of transient absorption by IO(v''=0). Equation E5, which includes only first order formation, was unable to fit the data and we were unable to extract any meaningful rates. This is likely due to the two distinct mechanisms involved in the formation of IO(v''=0), that are discussed more fully below.

Although not a major aim of this work, the IO(v''=1) loss rate has been measured as a function of total pressure from 50–150 Torr using conventional transient absorption and stepping the time delay between the photolysis and probe laser pulses. The total pressure was varied by increasing n_{N_2}, while holding the number densities of all other reactants constant. We assume that IO(v''=1) is lost by the bimolecular self-reaction and vibrational relaxation. The vibrational relaxation rate constant, $k_{v,1\rightarrow 0}$, was determined by fitting IO(v''=1) transient absorption traces, omitting the rapid rising edge, to the following expression:

$$n_{\mathrm{IO}}(t) = \frac{k'_{\mathrm{v},1\to0} n_{\mathrm{IO},0}}{k'_{\mathrm{v},1\to0} \exp\left(k'_{\mathrm{v},1\to0} t\right) - 2k_5 n_{\mathrm{IO},0} + 2k_5 n_{\mathrm{IO},0} \exp\left(k'_{\mathrm{v},1\to0} t\right)} + y \qquad \text{(E6)}$$

where k_5 is fixed at 9.9×10^{-11} cm^3 s^{-1}, $k'_{\mathrm{v},1\to0}$ is the pseudo-first order loss rate due to vibrational relaxation, and y accounts for any baseline offset.[34] IO(v''=1) was typically removed within 800 μs. A rate constant for IO(v''=1) vibrational relaxation of $k_{\mathrm{v},1\to0} = (1.6\pm0.4)\times10^{-15}$ cm^3 s^{-1} was obtained from the slope a linear plot of $k_{\mathrm{v},1\to0}'$ as a function of $n_{\mathrm{N_2}}$. This rate constant is in agreement with the rate constant of $k_{\mathrm{v},1\to0} = (1.9\pm0.4)\times10^{-15}$ cm^3 s^{-1} estimated by Gómez-Martin *et al*.[37] A zero-$n_{\mathrm{N_2}}$-limited rate of $(3.9\pm0.9)\times10^3$ s^{-1} was determined from the y-intercept of the linear fit, which is interpreted as the rate of vibrational relaxation by O_2 and residual CH_2I_2. The overall rate of vibrational relaxation is an order of magnitude slower than the apparent rate of IO(v''=0) formation, indicating that the vibrational ground state products are not a result of population cascading down from higher vibrational levels.

Pressure-dependence of IO formation rates

The results of a limited study of the dependence of the rates of formation of IO(v''=0) and IO(v''=1) on total pressure are shown in Figure 5. Measurements of the IO(v''=0) and IO(v''=1) formation rates were made using conventional transient absorption and SKaR methods as described previously. The total pressure was changed by varying $n_{\mathrm{N_2}}$ and holding all other reactant number densities constant. The data shown in Figure 5 were determined from experiments that used $n_{\mathrm{O_2}} = 5.4\times10^{16}$ cm^{-3} and 3.4×10^{17} cm^{-3}, when probing v''=0 and 1, respectively. While $k_{2a,0}$ is independent of total pressure over this range, $k_{2a,1}$ is strongly pressure dependent and decreases as the pressure is increased.

IO(v''=1) and IO(v''=0) yields

The maximum observed absorption coefficients for the (3,0) and (3,1) bands following 355 nm photolysis at 52±3 Torr and 20% O_2 are 2.16×10^{-5} cm^{-1} and 2.66×10^{-6} cm^{-1} at ~60 μs and ~6 μs after photolysis, respectively. Since loss rates of both vibrational levels are significantly slower than the formation rate, the peak absorption coefficients should be good approximations of the total populations formed in each vibrational level. However, the relative transition strengths of the A–X(3,0) and (3,1) bands are not well known. Previous measurements of the IO A–X absorption spectra that include hot bands have used the I + O_3 or O(^{3}P) + I_2 reactions to form IO.[37–39] The IO vibrational population distribution resulting from these reactions is not clearly defined, leading to large variability in the experimental absorption cross sections for the (3,1) band. Most recent estimates of absorption cross sections for the (3,1) band have assumed that it is diffuse, which is in disagreement with the high resolution studies in this work.[37] The experimentally determined absorption coefficients are weighted by their Franck-Condon factors in lieu of using absorption cross sections from the literature to compare the relative populations in v''=0 and 1.

Calculations to predict Franck-Condon factors for the IO A–X transition were carried out in LEVEL8 using potential curves derived using the Rydberg-Klein-Rees (RKR) method.[40,41] Dunham coefficients for IO in the $A^2\Pi_{3/2}$ and $X^2\Pi_{3/2}$ states were taken from Miller *et al.* and Newman *et al.*[30,42] Transition probabilities are directly proportional to the squares of the Franck-Condon factors, $\left|\langle\psi_{v',J'}|\psi_{v'',J''}\rangle\right|^2$, assuming the electronic transition dipole moment is constant. The calculated Franck-Condon factors (shown in Figure 6) are in fairly good agreement with those calculated previously by Rao *et al.*[43] using potentials defined by older spectroscopic constants; the calculated transition frequencies are generally within 1 cm^{-1} of those measured

experimentally.[30] The FCFs for the (3,0) and (3,1) bands are calculated to be 0.0958 and 0.1087, respectively, indicating that the transition probability is ~29% larger for the (3,1) band. Using a value of 3.24×10^{-17} cm^2 for the absorption cross section of the (3,0) band head at 435.72 nm from Spietz *et al*. (0.07 nm resolution),[38] we estimate a peak IO(v''=0) number density of approximately 4.2×10^{13} cm^{-3}, and consequently a yield of 0.10. After correcting for the slightly higher sensitivity for IO(v″=1), we estimate a peak number density of 4.0×10^{12} cm^{-3} and yield of only 0.01. The factor of ten greater yield of the vibrational ground state is surprising given that the apparent rate constant for formation of the IO(v''=0) is a factor of six smaller than that for IO(v''=1) and implies that an additional mechanism rapidly damps the buildup of IO(v''=1). The pressure dependence of $s_{2a,1}$ indicates that this is a collisional process. The small overall yield of IO in the reaction of $CH_2I + O_2$ observed in this work is consistent with previous measurements of large yields of I atoms from reaction (2b).[10,24] Measurements that probed IO directly have also found a relatively small overall yield.[12,13]

Discussion

The kinetics and mechanism of the reaction between CH_2I and O_2 has been the subject of some debate in the literature. Direct measurements of the total loss of CH_2I result in consistent measurements of k_2 in the range $1.4–1.6\times10^{-12}$ cm^3 s^{-1} and provide good upper limits for the individual rate constants associated with the various product pathways of reaction (2).[9,10] Measurements of the IO(v''=0) formation rate constant, however, have resulted in a broad range of rate constants for reaction (2a). Indeed, whether this mechanism proceeds via a direct[11,12] or indirect[14,25] mechanism is obscured by conflicting evidence.

Existing rate constants for the formation of IO(v''=0) from the reaction of $CH_2I + O_2$, including both direct and indirect formation models, range from 3.8×10^{-11} to 2.6×10^{-14} cm^3 s^{-1}. The

apparent rate constant reported here, $k_{2a,0}$ = 1.5±0.1×10^{-13} cm^3 s^{-1}, falls within the scope of values previously reported in the literature. However, the non-zero intercept observed in the linear fit of the IO(v''=0) formation rate as a function of n_{O_2} shown in Figure 3 indicates that IO(v''=0) is not, or at least not exclusively, formed directly via reaction (2a); it reflects the phenomenological dependence of the rate on n_{O_2} rather than a real bimolecular rate constant.

The temporal behavior of IO(v''=0) has been modeled numerically using a kinetic scheme that is similar to that proposed by Ting *et al.*[25] In the interests of simplicity, we choose to omit the CH_2IO_2 radical [formed in reaction (2c)] from the model. If CH_2IOO is formed at all under our experimental conditions, the yield is likely to be small and the subsequent chemistry relies heavily on estimated rate constants.[25] From an operational perspective, inclusion of CH_2IOO in the model was found to have a negligible effect on the IO temporal profiles. The reactions included in the simplest possible kinetic model are outlined below.

$CH_2I_2 + h\nu \rightarrow CH_2I + I$		(1)
$CH_2I + O_2 \rightarrow HCHO + IO(v''=0)$	$k_{2a,0} = \beta_0 k_2$	(2a)
$CH_2I + O_2 \rightarrow CH_2OO + I$	$k_{2b} = (1 - \beta_0) k_2$	(2b)
$CH_2OO + I \rightarrow HCHO + IO(v''=0)$	k_4	(4)
$IO + IO \rightarrow$ products	k_5	(5)
$I + I + M \rightarrow I_2 + M$	k_6	(6)
$CH_2OO + CH_2OO \rightarrow HCHO + HCHO + O_2$	k_7	(7)

CH_2I radicals are initially formed by photolysis and can react with O_2 either via reaction (2a) to form IO(v''=0) directly, controlled by the branching fraction β_0, or via reaction (2b) to form the

Criegee intermediate. We assume $k_2 = 1.4\times10^{-12}$ cm^3 s^{-1} following the experimental measurements of Eskola *et al.*[10] In addition to reaction (2a), IO(v''=0) radicals are formed by the secondary reaction between CH_2OO and I atoms, reaction (3). The rate constant for reaction (4) has not been measured directly, although Ting *et al.*[25] assumed a value of $k_4 = 9\times10^{-12}$ cm^3 s^{-1}, significantly larger than the predicted value of $k_4 = 5.5\times10^{-13}$ cm^3 s^{-1}, which was based on *ab initio* calculations.[26] Self-reactions (5), (6) and (7) act as irreversible sinks for IO, I and CH_2OO respectively and are modelled using rate constants of 9.9×10^{-11} cm^3 s^{-1},[33,34] 1×10^{-32} cm^6 s^{-2},[44] and 8×10^{-11} cm^3 s^{-1}.[25] All rate constants used in the model are summarized in Table 2.

Early-time IO profiles derived from this kinetic model are shown in Figure 7 alongside typical experimental data measured with O_2 fractions of 0.05, 0.10, and 0.15 of the total pressure. In Scheme I, the direct formation pathway is turned off by setting $\beta_0 = 0$, making sequential formation via reactions (2b) and (3) the sole source of IO(v''=0). This significantly underestimates the rate of IO(v''=0) formation and results in a profile shape that is qualitatively different from the experiment. Adjusting the estimated value of k_3 failed to improve the agreement with the experimental results. The direct formation pathway was turned on in Scheme II by adjusting the value of β_0; a value of $\beta_0 = 0.08$ was found to be optimal and qualitatively describes the very early time behavior, although obvious discrepancies still exist. The best agreement with the experimental data was found for Scheme II′ for which $\beta_0 = 0.12$ was assumed and the rate constant for reaction (4) was increased to $k_4 = 1.8\times10^{-11}$ cm^3 s^{-1}, a factor of two greater than the estimate of Ting *et al.*[25] The larger branching fraction required in this kinetic model implies that the bimolecular rate constant for direct production of IO(v''=0) is $k_{2a,0} = (1.7\pm0.2)\times10^{-13}$ cm^3 s^{-1}, which agrees with the phenomenological rate constant obtained from the data shown in Figure 2. The residual $k_{2b} = (1.23\pm0.15)\times10^{-12}$ cm^3 s^{-1} is also consistent with

previous direct measurements of the CH_2OO formation rate constant.[20,25]

In marked contrast to IO(v''=0), the kinetic data for formation of IO(v''=1), are consistent with direct formation by a bimolecular process involving O_2. The rate constant $k_{2a,1}$ = (9±1)×10^{-13} cm^3 s^{-1} is 5.3 times greater than the value of $k_{2a,0}$ inferred from modeling the reaction kinetics. The IO(v''=1) time profiles also peak at earlier times, consistent with the absence of the sequential formation mechanism involving reaction (4) that is important for formation of IO(v''=0).

The mechanism of formation for IO(v''=1) via reaction (2) has not been included in the kinetic model for several reasons. If production of IO(v''=1) is included as an additional pathway of reaction (2), the measured rate constant $k_{2a,1}$ would imply a branching fraction of β_1 = 0.64. The rate constant for CH_2OO production via reaction (2b) would be given by

$$k_{2b} = (1 - \beta_0 - \beta_1)k_2$$

A branching fraction of β=0.76 for production of IO in both v''=0 and 1 results in a value of k_{2b} that is significantly smaller than that determined by previous direct measurements of the Criegee intermediate formation rate (approximately 1.4–1.8×10^{-12} cm^3 s^{-1}).[9,10,17,25] Furthermore, this model would suggest that the reaction should produce significantly more IO radicals in v''=1 than in v''=0, in marked contrast to the experimentally observed peak absorption coefficients.

Even after allowing for the sequential mechanism, which accounts for around 65% of the total IO(v''=0) population (shown in Figure 7), there remains a strong propensity for production of IO(v''=0). The possibility that the rapid formation of IO(v''=1) is damped by an even faster loss process can also be discounted as under typical experimental conditions the loss rates for IO in v''=0 and v''=1 are broadly similar, and largely determined by the self-reaction. We are forced to

conclude that the reaction mechanisms that form IO(v''=0) and IO(v''=1) are decoupled, aside from vibrational relaxation induced by collisions with the bath gases which is sufficiently slow to have a negligible influence on the IO(v''=0) formation rate.

The apparent contradiction of small IO(v''=1) yield coupled to a much larger formation rate constant $k_{2a,1}$ can be qualitatively resolved by consideration of the internal energy distribution of the reactant CH_2I. Photolysis of CH_2I_2 produces highly internally excited CH_2I* radicals; at a photolysis wavelength of 355 nm, the average internal energy of the CH_2I fragment is $\langle E_{\mathrm{int}} \rangle =$ 21.7±3.0 kcal mol^{-1}.[45] One possible explanation for our experimental observation is that the highly internally excited CH_2I* radicals produced by photolysis react with O_2 to produce vibrationally excited IO radicals directly. If this is the case, the small yield of IO(v''=1) is controlled by the reaction being effectively quenched by collisional relaxation of CH_2I* reagent, consistent with the pressure-dependence of $k_{2a,1}$ Loss of the CH_2I* radical population, through reaction or collisional relaxation, effectively switches off the production of IO(v''=1), preventing the population increasing beyond that in v''=0. Once the CH_2I radicals are collisionally relaxed the reaction may proceed to form only IO(v''=0), either directly via reaction (2a) or sequentially via reactions (2b) and (4). There is, however, no *a priori* reason to expect the reaction of CH_2I* with O_2 to produce *exclusively* IO(v''=1). An alternative explanation, and one that is preferred, is that CH_2I* radicals are largely responsible for the direct reaction (2a), forming IO(v''=0,1) and HCHO; once relaxed, reaction (2b) dominates and forms exclusively IO(v''=0) via the sequential mechanism involving reaction (4). The very different time delays at which the maximum absorption coefficients are observed are consistent with the sequential mechanism producing no IO(v''=1). A CH_2I* reactant pool, that is collisionally relaxed to CH_2I, has not been included in the kinetic model described earlier, because there are no reported measurements for relaxation of

CH_2I^* by N_2 or O_2, which are the major components of the gas mixture. Rates of collisional relaxation of CH_2I^* by CH_2I_2 have been found to be rapid,[46] while Ar is a significantly less efficient quencher.[47] Nonetheless, a rate constant within the observed range predicts a lifetime for CH_2I^* on the order of a few μs, which is consistent with the rise time observed for IO(v''=1) products. Most likely, the addition of this product channel to the kinetic model would require a modest reduction in the value of β_0 to restore agreement with the experimental data. The current model, however, already requires several estimated rate constants and it seems unlikely that much new insight would be gained by inclusion of additional estimated parameters to allow for collisional relaxation of CH_2I^*. More fundamentally, the rate constants and branching between various pathways may depend more subtly on the internal energy distribution of the CH_2I reactant.

The effect of "hot" molecules reacting prior to collisional thermalization on product branching has been suggested previously in studies of the OH + acetylene reaction.[48] While this is unlikely to have a profound effect on reaction (2) under atmospheric conditions, the mechanism of CH_2I radical production could have significant impact on laboratory studies of the $CH_2I + O_2$ reaction. Photolysis wavelengths of 266 nm (Nd:YAG 4th harmonic) or 248 nm (KrF excimer laser) have been used by other groups to photodissociate the CH_2I_2 precursor. At these wavelengths, the nascent CH_2I internal energy distributions are bimodal, resulting from the formation of both ground and spin-orbit excited iodine atoms, and centered around energies of 46.5 and 26.1 kcal mol^{-1} (266 nm) and 53.9 and 33.7 kcal mol^{-1} (248 nm). The details of the initial CH_2I^* internal energy distribution could have a particularly important consequence for studies performed under conditions where reaction rates are competitive with relaxation rates; it may not be safe to assume that reactant species are completely thermalized prior to reacting.

Experiments are currently underway to characterize the photolysis energy dependence of the formation kinetics of IO in v''=0 and 1, and to treat the relaxation of CH_2I* using detailed master equation modeling.

Conclusion

The kinetics of the production of IO in the reaction of CH_2I with O_2 has been studied using time-resolved cavity ring-down spectroscopy following 355 nm photolysis of CH_2I_2. We conclude that IO(v''=0) is produced primarily from secondary chemistry but also through a minor direct channel that contributes at early times. IO(v''=1) is formed exclusively directly with a rate constant that is over five times larger than that for IO(v''=0), yet the maximum vibrationally excited population is significantly smaller than that of the ground state. It is proposed that the direct production of IO radicals requires the reaction to involve CH_2I with some degree of internal excitation; as collisions and reactions remove the internally excited CH_2I* population, the direct reaction is quenched and the slower sequential mechanism continues to result in predominantly IO(v''=0).

Acknowledgements

We gratefully acknowledge YiTien Jou for her contribution to early stages of the development of the cavity ring-down apparatus.

References

(1) Carpenter, L. J. Iodine in the Marine Boundary Layer. *Chem. Rev.* **2003**, *103*, 4953–4962.

(2) Saiz-Lopez, A.; Plane, J. M. C.; Baker, A. R.; Carpenter, L. J.; Glasow, R. von; Gómez Martín, J. C.; McFiggans, G.; Saunders, R. W. Atmospheric Chemistry of Iodine. *Chem. Rev.* **2012**, *112*, 1773–1804.

(3) Jimenez, J. L.; Bahreini, R.; Cocker, D. R.; Zhuang, H.; Varutbangkul, V.; Flagan, R. C.;

Seinfeld, J. H.; O'Dowd, C. D.; Hoffmann, T. New Particle Formation from Photooxidation of Diiodomethane (CH_2I_2). *J. Geophys. Res. Atmospheres* **2003**, *108*, 4318.

(4) McFiggans, G.; Plane, J. M. C.; Allan, B. J.; Carpenter, L. J.; Coe, H.; O'Dowd, C. A Modeling Study of Iodine Chemistry in the Marine Boundary Layer. *J. Geophys. Res.* **2000**, *105*, 14371.

(5) Nakano, Y.; Enami, S.; Nakamichi, S.; Aloisio, S.; Hashimoto, S.; Kawasaki, M. Temperature and Pressure Dependence Study of the Reaction of IO Radicals with Dimethyl Sulfide by Cavity Ring-Down Laser Spectroscopy. *J. Phys. Chem. A* **2003**, *107*, 6381–6387.

(6) Roehl, C. M.; Burkholder, J. B.; Moortgat, G. K.; Ravishankara, A. R.; Crutzen, P. J. Temperature Dependence of UV Absorption Cross Sections and Atmospheric Implications of Several Alkyl Iodides. *J. Geophys. Res.* **1997**, *102*, 12819–12829.

(7) Mössinger, J. C.; Shallcross, D. E.; Cox, R. A. UV-VIS Absorption Cross-Sections and Atmospheric Lifetimes of CH_2Br_2, CH_2I_2 and CH_2BrI. *J. Chem. Soc. Faraday Trans.* **1998**, *94*, 1391–1396.

(8) Ayhens, Y. V.; Nicovich, J. M.; McKee, M. L.; Wine, P. H. Kinetic and Mechanistic Study of the Reaction of Atomic Chlorine with Methyl Iodide over the Temperature Range 218−694 K. *J. Phys. Chem. A* **1997**, *101*, 9382–9390.

(9) Masaki, A.; Tsunashima, S.; Washida, N. Rate Constants for Reactions of Substituted Methyl Radicals (CH_2OCH_3, CH_2NH_2, CH_2I, and CH_2CN) with O_2. *J. Phys. Chem.* **1995**, *99*, 13126–13131.

(10) Eskola, A. J.; Wojcik-Pastuszka, D.; Ratajczak, E.; Timonen, R. S. Kinetics of the Reactions of CH_2Br and CH_2I Radicals with Molecular Oxygen at Atmospheric Temperatures. *Phys. Chem. Chem. Phys.* **2006**, *8*, 1416–1424.

(11) Enami, S.; Ueda, J.; Goto, M.; Nakano, Y.; Aloisio, S.; Hashimoto, S.; Kawasaki, M. Formation of Iodine Monoxide Radical from the Reaction of CH_2I with O_2. *J. Phys. Chem. A* **2004**, *108*, 6347–6350.

(12) Enami, S.; Sakamoto, Y.; Yamanaka, T.; Hashimoto, S.; Kawasaki, M.; Tonokura, K.; Tachikawa, H. Reaction Mechanisms of IO Radical Formation from the Reaction of CH_3I with Cl Atom in the Presence of O_2. *Bull. Chem. Soc. Jpn.* **2008**, *81*, 1250–1257.

(13) Dillon, T. J.; Tucceri, M. E.; Sander, R.; Crowley, J. N. LIF Studies of Iodine Oxide Chemistry. *Phys. Chem. Chem. Phys.* **2008**, *10*, 1540–1554.

(14) Gravestock, T. J.; Blitz, M. A.; Bloss, W. J.; Heard, D. E. A Multidimensional Study of the Reaction CH_2I+O_2: Products and Atmospheric Implications. *ChemPhysChem* **2010**,

11, 3928–3941.

(15) Sehested, J.; Ellermann, T.; Nielsen, O. J. A Spectrokinetic Study of CH_2I and CH_2IO_2 Radicals. *Int. J. Chem. Kinet.* **1994**, *26*, 259–272.

(16) Lee, E. P. F.; Mok, D. K. W.; Shallcross, D. E.; Percival, C. J.; Osborn, D. L.; Taatjes, C. A.; Dyke, J. M. Spectroscopy of the Simplest Criegee Intermediate CH_2OO: Simulation of the First Bands in Its Electronic and Photoelectron Spectra. *Chem. – Eur. J.* **2012**, *18*, 12411–12423.

(17) Sheps, L. Absolute Ultraviolet Absorption Spectrum of a Criegee Intermediate CH_2OO. *J. Phys. Chem. Lett.* **2013**, *4*, 4201–4205.

(18) Ting, W.-L.; Chen, Y.-H.; Chao, W.; Smith, M. C.; Lin, J. J.-M. The UV Absorption Spectrum of the Simplest Criegee Intermediate CH_2OO. *Phys. Chem. Chem. Phys.* **2014**, *16*, 10438–10443.

(19) Taatjes, C. A.; Meloni, G.; Selby, T. M.; Trevitt, A. J.; Osborn, D. L.; Percival, C. J.; Shallcross, D. E. Direct Observation of the Gas-Phase Criegee Intermediate (CH_2OO). *J. Am. Chem. Soc.* **2008**, *130*, 11883–11885.

(20) Welz, O.; Savee, J. D.; Osborn, D. L.; Vasu, S. S.; Percival, C. J.; Shallcross, D. E.; Taatjes, C. A. Direct Kinetic Measurements of Criegee Intermediate (CH_2OO) Formed by Reaction of CH_2I with O_2. *Science* **2012**, *335*, 204–207.

(21) Su, Y.-T.; Huang, Y.-H.; Witek, H. A.; Lee, Y.-P. Infrared Absorption Spectrum of the Simplest Criegee Intermediate CH_2OO. *Science* **2013**, *340*, 174–176.

(22) McCarthy, M. C.; Cheng, L.; Crabtree, K. N.; Martinez, O.; Nguyen, T. L.; Womack, C. C.; Stanton, J. F. The Simplest Criegee Intermediate ($H_2C{=}O{-}O$): Isotopic Spectroscopy, Equilibrium Structure, and Possible Formation from Atmospheric Lightning. *J. Phys. Chem. Lett.* **2013**, *4*, 4133–4139.

(23) Stone, D.; Blitz, M.; Daubney, L.; Ingham, T.; Seakins, P. CH_2OO Criegee Biradical Yields Following Photolysis of CH_2I_2 in O_2. *Phys. Chem. Chem. Phys.* **2013**, *15*, 19119–19124.

(24) Huang, H.; Eskola, A. J.; Taatjes, C. A. Pressure-Dependent I-Atom Yield in the Reaction of CH_2I with O_2 Shows a Remarkable Apparent Third-Body Efficiency for O_2. *J. Phys. Chem. Lett.* **2012**, *3*, 3399–3403.

(25) Ting, W.-L.; Chang, C.-H.; Lee, Y.-F.; Matsui, H.; Lee, Y.-P.; Lin, J. J.-M. Detailed Mechanism of the $CH_2I + O_2$ Reaction: Yield and Self-Reaction of the Simplest Criegee Intermediate CH_2OO. *J. Chem. Phys.* **2014**, *141*, 104308.

(26) Su, Y.-T.; Lin, H.-Y.; Putikam, R.; Matsui, H.; Lin, M. C.; Lee, Y.-P. Extremely Rapid

Self-Reaction of the Simplest Criegee Intermediate CH_2OO and Its Implications in Atmospheric Chemistry. *Nat. Chem.* **2014**, *6*, 477–483.

(27) Roehl, C. M.; Burkholder, J. B.; Moortgat, G. K.; Ravishankara, A. R.; Crutzen, P. J. Temperature Dependence of UV Absorption Cross Sections and Atmospheric Implications of Several Alkyl Iodides. *J. Geophys. Res.* **1997**, *102*, 12819.

(28) O'Keefe, A.; Deacon, D. A. G. Cavity Ring-down Optical Spectrometer for Absorption Measurements Using Pulsed Laser Sources. *Rev. Sci. Instrum.* **1988**, *59*, 2544–2551.

(29) Wheeler, M. D.; Newman, S. M.; Orr-Ewing, A. J.; Ashfold, M. N. R. Cavity Ring-down Spectroscopy. *J. Chem. Soc. Faraday Trans.* **1998**, *94*, 337–351.

(30) Newman, S. M.; Howie, W. H.; Lane, I. C.; Upson, M. R.; Orr-Ewing, A. J. Predissociation of the $A^2\Pi_{3/2}$ State of IO Studied by Cavity Ring-down Spectroscopy. *J. Chem. Soc. Faraday Trans.* **1998**, *94*, 2681–2688.

(31) PGOPHER, a Program for Simulating Rotational Structure, C. M. Western, University of Bristol, http://pgopher.chm.bris.ac.uk.

(32) Bekooy, J. P.; Meerts, W. L.; Dymanus, A. High-Resolution Laser-Rf Spectroscopy on the $A^2\Pi_{3/2}$–$X^2\Pi_{3/2}$ System of Lodine Oxide (IO). *J. Mol. Spectrosc.* **1983**, *102*, 320–343.

(33) Bloss, W. J.; Rowley, D. M.; Cox, R. A.; Jones, R. L. Kinetics and Products of the IO Self-Reaction. *J. Phys. Chem. A* **2001**, *105*, 7840–7854.

(34) Harwood, M. H.; Burkholder, J. B.; Hunter, M.; Fox, R. W.; Ravishankara, A. R. Absorption Cross Sections and Self-Reaction Kinetics of the IO Radical. *J. Phys. Chem. A* **1997**, *101*, 853–863.

(35) Brown, S. S.; Ravishankara, A. R.; Stark, H. Simultaneous Kinetics and Ring-down: Rate Coefficients from Single Cavity Loss Temporal Profiles. *J. Phys. Chem. A* **2000**, *104*, 7044–7052.

(36) Brown, S. S.; Ravishankara, A. R.; Stark, H. Simultaneous Kinetics and Ring-down: Rate Coefficients from Single Cavity Loss Temporal Profiles. *J. Phys. Chem. A* **2000**, *104*, 8600–8600.

(37) Carlos Gómez Martín, J.; Spietz, P.; Burrows, J. P. Spectroscopic Studies of the I_2/O_3 Photochemistry: Part 1: Determination of the Absolute Absorption Cross Sections of Iodine Oxides of Atmospheric Relevance. *J. Photochem. Photobiol. Chem.* **2005**, *176*, 15–38.

(38) Spietz, P.; Gómez Martín, J. C.; Burrows, J. P. Spectroscopic Studies of the I_2/O_3 Photochemistry: Part 2. Improved Spectra of Iodine Oxides and Analysis of the IO Absorption Spectrum. *J. Photochem. Photobiol. Chem.* **2005**, *176*, 50–67.

(39) Laszlo, B.; Kurylo, M. J.; Huie, R. E. Absorption Cross Sections, Kinetics of Formation, and Self-Reaction of the IO Radical Produced via the Laser Photolysis of $N_2O/I_2/N_2$ Mixtures. *J. Phys. Chem.* **1995**, *99*, 11701–11707.

(40) LeRoy, R. Level 8.0: A Computer Program for Solving the Radial Schrodinger Equation for Bound and Quasibound Levels. *Univ. Waterloo Chem. Phys. Rep. CP-663* **2012**.

(41) LeRoy, R. RKR1 2.0: A Computer Program Implementing the First-Order RKR Method for Determining Diatomic Molecule Potential Energy Functions. *Univ. Waterloo Chem. Phys. Rep. CP-425* **1992**.

(42) Miller, C. E.; Cohen, E. A. Rotational Spectroscopy of IO $X^2\Pi_i$. *J. Chem. Phys.* **2001**, *115*, 6459–6470.

(43) Rao, M. L. P.; Rao, D. V. K.; Rao, P. T. Dissociation Energies, R-Centroids and Franck-Condon Factors of IO Molecule. *Phys. Lett. A* **1974**, *50*, 341–342.

(44) Russell, K. E.; Simons, J. Studies in Energy Transfer. I. The Combination of Iodine Atoms. *Proc. R. Soc. Math. Phys. Eng. Sci.* **1953**, *217*, 271–279.

(45) Toulson, B. W.; Alaniz, J. P.; Foreman, E. S.; Murray, C.; Hill, J. G. Photodissociation Dynamics of CH_2I_2 in the near UV. **in preparation**.

(46) Lenzer, T.; Oum, K.; Schroeder, J.; Sekiguchi, K. Gas-Phase Collisional Relaxation of the CH_2I Radical after UV Photolysis of CH_2I_2. *J. Phys. Chem. A* **2005**, *109*, 10824–10831.

(47) Baughcum, S. L.; Leone, S. R. Photofragmentation Infrared Emission Studies of Vibrationally Excited Free Radicals CH_3 and CH_2I. *J. Chem. Phys.* **1980**, *72*, 6531–6545.

(48) Glowacki, D. R.; Lockhart, J.; Blitz, M. A.; Klippenstein, S. J.; Pilling, M. J.; Robertson, S. H.; Seakins, P. W. Interception of Excited Vibrational Quantum States by O_2 in Atmospheric Association Reactions. *Science* **2012**, *337*, 1066–1069.

Figures

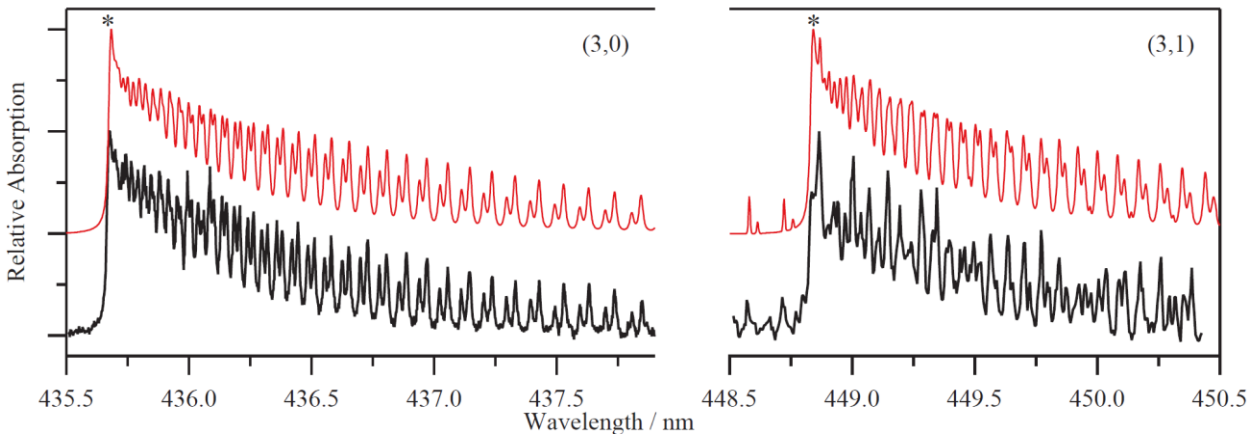

Figure 1. CRD spectra of the A–X (3,0) [left] and (3,1) [right] bands of IO. Experimental spectra are shown in black and the accompanying simulations are shown in red and offset for clarity.

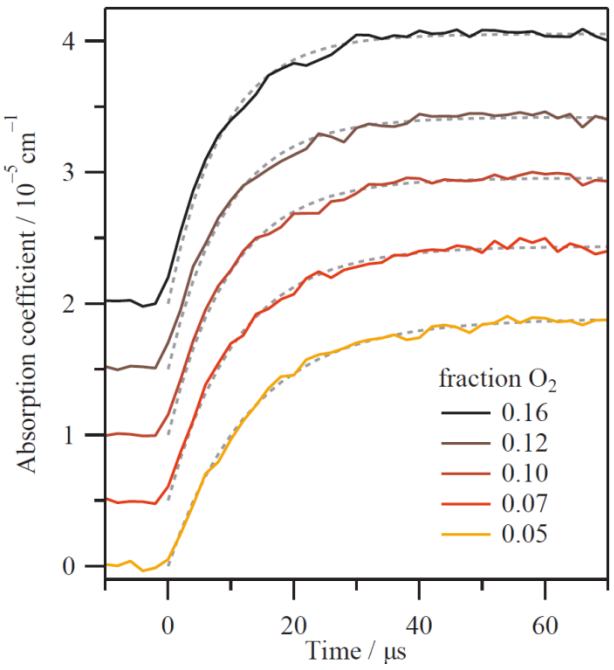

Figure 2. Kinetic profiles for IO(v''=0) monitored with the probe laser wavelength tuned to the $A^2\Pi_{3/2}$–$X^2\Pi_{3/2}$ (3,0) band head at a total pressure of 52 Torr and a range of O_2 fractions.

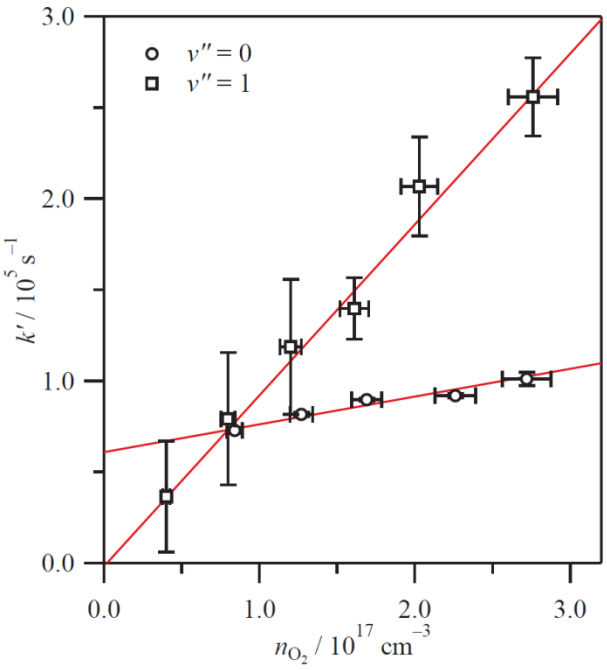

Figure 3. Pseudo-first order kinetic plots of rates measured from transient absorption experiments for IO (v''=0) and SKaR experiments for IO (v''=1) as a function of O_2 number density. Error bars represent 1σ uncertainties.

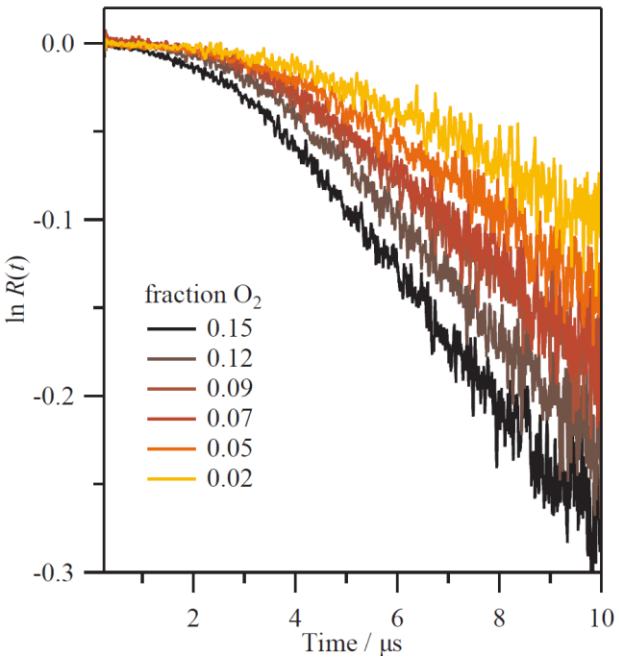

Figure 4. Sample SKaR profiles for IO(v''=1) monitored at the $A^2\Pi_{3/2}$–$X^2\Pi_{3/2}$ (3,1) band head at a total pressure of 52 Torr and a range of O_2 fractions.

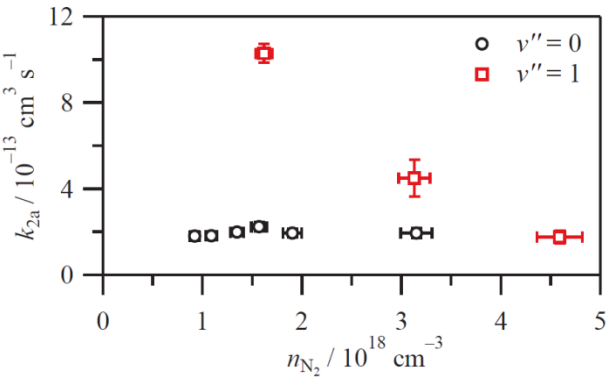

Figure 5. Pressure dependence of the bimolecular rate constants k_{2a} for formation of IO(v''=1) and IO(v''=0) determined from SKaR and conventional transient absorption spectroscopy, respectively.

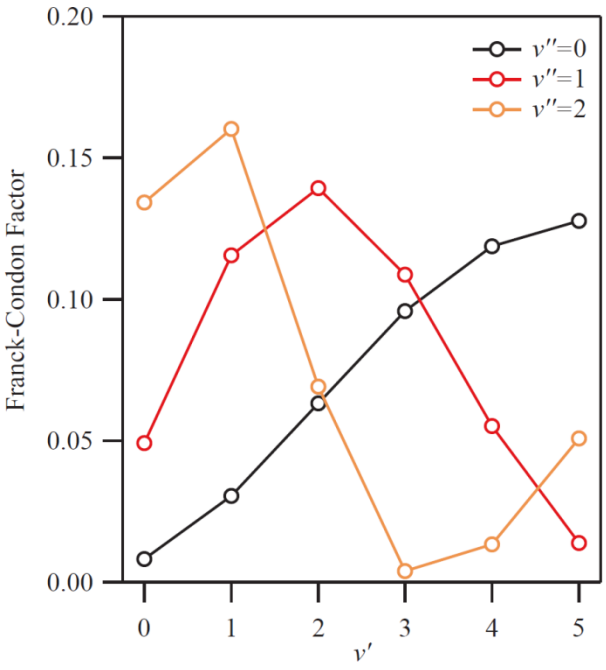

Figure 6. Franck-Condon factors for A−X(v',v'') bands.

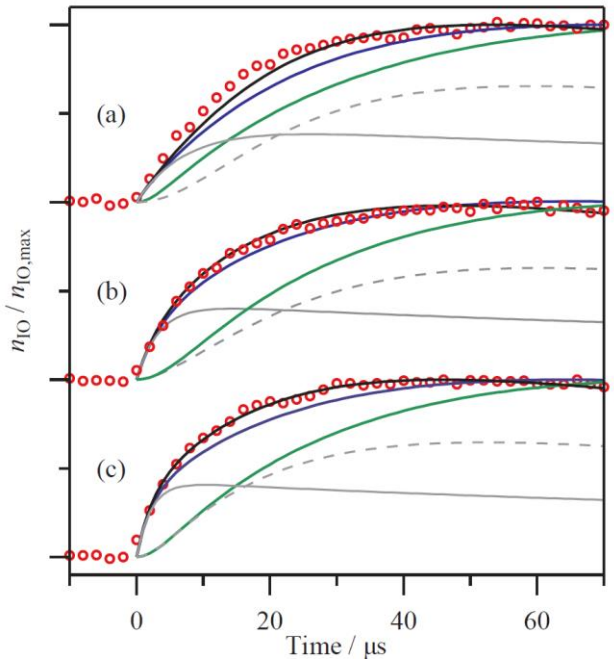

Figure 7. Experimental (circles) and modelled IO time profiles (lines) at a) 0.06 O_2 fraction, b) 0.10 O_2 fraction, and c) 0.15 O_2 fraction. Scheme I (green) includes only sequential, indirect formation of IO i.e. the branching fraction β_0 =0. Scheme II (blue) includes a direct pathway with β_0 = 0.08. Scheme II′ (black) uses β_0 = 0.12 and $k_4 = 1.8\times10^{-11}$ cm^3 s^{-1}. Contributions to the total IO signal from indirect formation (dashed gray) and a direct channel (solid gray) under Scheme II′ are also shown.

Tables

Table 1. IO formation and vibrational relaxation rate constants determined in this work.

Reaction	Rate constant	k / 10^{-13} cm^3 s^{-1}
$CH_2I + O_2 \rightarrow HCHO + IO(v''=0)^{\dagger}$	$k_{2a,0}$	1.5±0.1
$CH_2I + O_2 \rightarrow HCHO + IO(v''=0)$	$k_{2a,0} = \beta_0 k_2$	1.7±0.2
$CH_2I + O_2 \rightarrow HCHO + IO(v''=1)$	$k_{2a,1}$	9±1
$IO(v''=1) + N_2 \rightarrow IO(v''=0) + N_2$	$k_{v,1\rightarrow0}$	(1.6±0.4)×10^{-2}

Table 2: Summary of rate constants used in the kinetic model.

Reaction	k / cm^3 s^{-1}	Reference
2	1.4×10^{-12}	Eskola *et al.*[10]
4	9×10^{-12}‡	Ting *et al.*[25]
5	9.9×10^{-11}	Harwood *et al.*,[34] Bloss *et al.*[33]
6	1.9×10^{-14}§	Russell and Simons[44]
7	8×10^{-11}	Ting *et al.*[25]

† Value determined from linear dependence of apparent first order rate on n_{O_2}.
‡ This value is doubled to 1.8×10^{-11} cm^3 s^{-1} in Scheme II′.
§ Assuming $n_M = 1.7\times10^{18}$ cm^{-3}; third order rate constant is 1×10^{32} cm^6 s^{-1}.